



Box–Behnken design-based optimization for biodiesel production from waste cooking oil using Mahogany (*Swietenia macrophylla*) fruit shell derived activated carbon as a heterogeneous base catalyst

Mosharof Hossain^{1,2} · Lipiar Khan Mohammad Osman Goni² · Nuzhat Muntaha² · Mohammad Shah Jamal² · Shah Mohammad Asaduzzaman Sujan² · Shamim Ahmed³ · Dipa Islam⁴ · Riyadh Hossen Bhuiyan⁵ · Abu Naieum Muhammad Fakhruddin¹

Received: 6 February 2021 / Accepted: 15 May 2021 / Published online: 21 May 2021
© Akadémiai Kiadó, Budapest, Hungary 2021

Abstract

In this study, activated carbon was derived from inexpensive and abundant biomass feedstock Mahogany fruit shell and activated with KOH to act as a heterogeneous base catalyst for transesterification of waste cooking oil to biodiesel. The catalyst was characterized by means of FT-IR, XRD, FESEM-EDS and particle size analysis techniques. Box–Behnken design optimization was carried out to study the complex interaction between reaction parameters. Catalyst concentration, methanol to oil molar ratio, and reaction time were varied from 0.5–2 wt%, 6:1–12:1, and 120–240 min, to obtain the maximum biodiesel conversion. Reaction parameters with the combination of 2 wt% catalyst concentration, 180 min reaction time, 12:1 methanol to oil molar ratio, and 65 °C temperature led to the best yield of 97.26%. The optimization study revealed methanol to oil molar ratio to be the most influential parameter to dictate the biodiesel conversion. High coefficient of determination (R^2) value of 99.844% proved that the predicted biodiesel yields were very close to the experimental ones. Gas chromatography (GC) analysis disclosed methyl palmitate (41.18%) and methyl oleate (48.19%) to be the major composition of the synthesized biodiesel. Physicochemical properties of the biodiesel, such as viscosity (4.58 cSt), density (862 kg/m³), acid value (0.28 mg KOH/g), pour point (16 °C), and flash point (128 °C) were measured and found to be in compliance with the standards. The maximum yield coming from a quite low catalyst concentration and methanol to oil molar ratio is phenomenal from an industrial perspective.

Keywords Activated carbon · Biodiesel · Box–Behnken design · Mahogany · Transesterification · Waste cooking oil

✉ Mosharof Hossain
mosharof@bcsir.gov.bd

Extended author information available on the last page of the article

Introduction

Fossil fuels or non-renewable energy resources—coal, gas and crude oil—are the cardinal sources of world energy supply. However, an econometrics model developed by Shafiee and Topal [1] showed that coal is the only fossil fuel remaining after 2042. On the contrary, harmful chemical substances, such as carbon dioxide, greenhouse gases, and other organic compounds are released when fossil fuels are burnt [2, 3]. Therefore, a foreseeable future with a scarcity of fossil fuels and current environmental issues caused by the same energy sources have made the search for renewable and clean energy sources highly worthwhile [4–6]. Recently, biodiesel—consisting of fatty acid methyl esters (FAME)—has gained considerable attention because of its renewable, biodegradable, non-toxic, and less pollutant emitting nature [7–14] and functional properties similar to petrodiesel [15]. Biodiesel's greater ability, in contrast with petrodiesel, to abate greenhouse gas emissions has made it the Environmental Protection Agency (EPA) certified first and main commercial-scale advanced biofuel [16]. To add to its advantages, biodiesel can be easily derived from vegetable oils, animal fats, and waste cooking oils (WCO) [17]. Nevertheless, the high free fatty acid (FFA) content of animal fats and non-edible vegetable oils render their use expensive because of requiring double-step reaction (esterification and transesterification) in order for the conversion of triglycerides (TAG) into biodiesel. On the other hand, the high cost associated with edible oils and their role in battling hunger and starvation worldwide make their use for transesterification quite impractical [18]. WCO's relatively lower FFA content and high abundance make it an ideal feedstock for biodiesel production [19]. 15 million tons of WCO that could be used as feedstock are thrown into the water and land across the globe [20]. Thus, the conversion of low-cost and easily available WCO to biodiesel is the most economical and sustainable option.

Among several methods, for instance, dilution with hydrocarbons, pyrolysis, and emulsification, production of FAME via the catalytic transesterification of TAG with methanol is the most economical and easy one [9, 21]. Biodiesel produced via catalytic transesterification has been reported to be of relatively lower viscosity that prevents incomplete combustion leading to better engine performance [10]. However, the heterogeneous catalysts are preferred to the homogeneous ones for several reasons, such as environmental safety, skipping the step of crude ester washing, ease of separation, catalyst reusability, lower energy consumption, insensitivity to acidity value, preventing soap formation and hydrolysis while using WCO as feedstock, and the lower catalyst requirement [22–24]. Biodiesel production using oxides, mixed oxides, hydrotalcite, zeolites, and supported alkali metals as heterogeneous catalysts has gained widespread popularity [25]. Recently, catalyst carriers derivation from agricultural residues and bio-wastes, such as calcium oxide from shells [26] and sodium silicate from rice husk [27] have gained popularity for biodiesel production. Activated carbon (AC) is another very cheap and efficient carrier for both enzymatic and chemical catalysis. Carbonaceous materials, namely coal, wood, and biomass sources can be

activated—either chemically or physically—to produce AC [11]. AC's high catalytic activity, highly porous and heat and radiation resistant natures make them really suitable and highly effective for the transesterification of TAG [28, 29]. In this study, AC was prepared from cheap and readily available Mahogany (*Swietenia macrophylla*) fruit shell (MFS) by means of chemical activation using potassium hydroxide and used it thereafter for the esterification of WCO to biodiesel. Mahogany—belonging to the Meliaceae family and very popular for its wood and several medicinal uses—is found in many areas across the globe but predominantly in Asia and the Middle East [30–32].

One factor at a time (OFAT)—a widely used traditional method of process optimization—requires a huge pool of experiments to find the optimal points, rendering the whole process both economically unfeasible and time-consuming [19, 33]. Furthermore, the possibility of more than one factor influencing the system simultaneously will make the achievement of the true optimal condition highly unlikely [34]. To overcome the drawbacks of these OFAT-mediated issues, Box–Behnken design (BBD)-based response surface methodology (RSM)—a powerful optimization tool—was introduced to study the interaction between process variables. There are a couple of evidences on the derivation of AC from Mahogany fruit husk [35] or shell [36] and Mahogany seed waste [31]. There are also numerous reports on the production of biodiesel from WCOs [37–40], edible oils [8, 12, 26, 41], and non-edible oils [10, 13, 42] using AC as heterogeneous catalyst support. However, to the best of our knowledge, MFS derived AC has not yet been exploited as a catalyst support for transesterification of any type of oils. In this report, MFS derived AC has been proved to have acted as an efficient support for KOH loading to synthesize biodiesel from waste cooking palm oil with excellent yield, with the experimental design being inspired by BBD-based RSM.

Experimental

Chemicals and materials

Mahogany fruits were collected from BCSIR, Dhaka. WCO oil was obtained from a local restaurant. Hydrochloric acid (HCl) was purchased from Sigma-Aldrich, UK. Potassium hydroxide (KOH) and methanol (CH₃OH) were purchased from Merck, Germany. Chemicals used throughout the investigation were of analytical grade and used as received.

Catalyst preparation

AC was synthesized by slightly varying the method developed by Roschat et al. [27]. Firstly, MFS were broken down into smaller pieces and washed with distilled water to remove any dirt and impurities. These small pieces were then blended and dried in an oven at 105 °C for 24 h. The blended MFS were then ball milled (PULVERISETTE, FRITSCH, Germany) into fine powdery particles. Ball

milled MFS powders were pretreated with 1 M HCl at 80 °C for 6 h in a water-bath to serve the purpose of acid digestion. Subsequently, the HCl-pretreated slurry was filtered and washed with distilled water until the filtrate turned neutral and finally washed three more times with deionized water. The filtered product was then kept in an oven at 105 °C for overnight drying. The dried powders were carbonized afterward at 700 °C for 4 h in a tubular furnace (Nabertherm, Germany) under N₂ flow. The obtained biochar (MFSAC) was then treated with KOH pellets (1:1, wt/wt) in an amount of deionized water that was just enough to dissolve the KOH pellets and soak the biochar at the same time. The heterogeneous mixture was then stirred at 30 °C for 30 min following an overnight drying at 105 °C. Finally, the KOH impregnated biochar was activated at 850 °C for 2 h using the same tubular furnace under N₂ flow. The final product—MFSAC-KOH (KOH impregnated activated carbon)—was sealed in a vial and stored in a desiccator until further use.

Catalyst characterization

The surface morphology of MFSAC and MFSAC-KOH was observed by employing field emission scanning electron microscopy (FESEM; JSM-7610F, JEOL, Japan) (accelerating voltage: 15 kV, magnification: 15000X). Energy dispersive spectroscopy (EDS; 7610F, JEOL, Japan) (accelerating voltage: 15 kv, magnification: 500X), coupled with FESEM, was used to identify the presence of corresponding elements in MFSAC and MFSAC-KOH samples. X-ray diffractometer (XRD; Bruker D8 Advance, Germany)—attached with Cu-K α radiation ($\lambda=0.15405$ nm)—was utilized to find the crystalline phases and diffraction peaks of MFSAC and MFSAC-KOH using electron beam generated at 40 mA and 40 kV. The diffraction data were recorded in the scanning angle (2θ) range of 0–90° with the step size and scan time being 1.120° and 30 s per step. Fourier transform-infrared spectroscopy (FTIR; Frontier, PerkinElmer, UK) study was performed to characterize various surface functionalities in MFS, MFSAC and MFSAC-KOH samples, with wavenumbers ranging from 380 to 4000 cm⁻¹. Particle size distributions and specific surface area of MFSAC and MFSAC-KOH samples were measured by a Mastersizer 3000 laser diffraction analyzer (Malvern Panalytical Ltd, Malvern, UK). The particles were suspended in deionized water (refractive index: 1.330) while the particle refractive index was set to be 2.420.

Waste cooking oil purification and characterization

The collected WCO was filtered first to eradicate suspended food particles or solid impurities. It was then placed in an oven at 105 °C for 30 min to remove moisture. The WCO was titrated against 0.1 N KOH to determine its FFA content. Since the FFA content of the used WCO was way below 2% (0.33% precisely), no pretreatment/esterification of the WCO was necessary.

Transesterification of waste cooking oil

The transesterification reactions were performed in three-neck round-bottom flasks (RBF). Reaction temperature, stirring speed, and weight of WCO for all of the studied reactions were fixed to be 65 °C, 600 rpm, and 5 g. First, purified WCO and a magnetic stirrer were put into the RBF. Appropriate amounts (determined by Box–Behnken statistical design discussed later) of MFSAC-KOH catalyst and methanol were added to the WCO in the RBF for each of the studied reaction. Afterward, the RBF was fitted with a water reflux condensation facility and thermometer and immersed in a water bath on top of a stirring hot plate. Stirring and reaction time count were initiated after the temperature of the reaction vessel had reached 65 °C, and the temperature throughout the studied reactions were maintained to be at 65 ± 2 °C. After the reactions were completed, the mixtures were transferred into a separatory funnel and kept for 24 h. Two distinct layers of FAME (upper layer; yellowish) and glycerol (middle layer; brownish) were produced. The FAME portion was collected into a 20 ml vial and kept in an oven at 105 °C for 30 min to remove any moisture and unreacted methanol since they have been reported to have caused the growth of biological organisms, increase of the acid value of fuel and lessening of the flash point of fuel [10]. The vial was sealed afterward and stored for further analysis. The conversion (%) of the transesterification reactions was calculated with the help of nuclear magnetic resonance spectroscopy (NMR; Bruker 400™ ASCEND, Germany) following a straightforward equation (Eq. 1) developed by Gelbard et al. [43], in which C is the percentage yield of corresponding FAME from TAG feedstock. A_{ME} and $A_{\alpha-CH_2}$ represent the integration value of the protons of the methyl esters and methylene protons having a strong singlet peak and triplet peak at 3.64 ppm and 2.29 ppm.

$$C(\%) = 100 \times (2A_{ME}/3A_{\alpha-CH_2}) \quad (1)$$

Gas chromatography analysis of biodiesel.

FAME composition was determined by gas chromatography (GC; Agilent 6890N, USA) according to EN 14103. The GC was equipped with a flame ionization detector (FID), and the sample was run through an Agilent HP-1 GC column (60 m × 0.25 mm × 0.25 μm).

Experimental design

BBD was utilized to gain insight into the interaction of transesterification reaction's process parameters leading to maximum response, i.e., biodiesel conversion. The impact of three reaction variables—A: catalyst concentration (wt%), B: methanol to oil ratio (mol:mol), and C: reaction time (min)—on the response transesterification conversion was evaluated through regression and graphical analysis. The stirring

Table 1 Selected variables and coded levels used in the BBD

Variables	Symbol	Coded levels		
		− 1	0	+ 1
Catalyst amount (wt%)	A	0.5	1.25	2
Methanol:oil (mol:mol)	B	6:1	9:1	12:1
Reaction time (min)	C	120	180	240

speed and reaction temperature for all the studied reactions were fixed to be 600 rpm and 65 °C. A total of 15 reactions were done separately with a view to obtaining the experimental response of biodiesel yield. The coded and uncoded levels of the independent reaction variables used for the transesterification of WCO are shown in Table 1.

Statistical analysis

Minitab statistical software (Minitab, LLC, Pennsylvania, USA) was used for the purpose of executing regression and graphical analysis. The maximum values of biodiesel yield were considered as the response of the design experiment for the transesterification process. The experimental data obtained from the whole set of experiments were analyzed by means of the following second-order polynomial equation (Eq. 2).

$$Y_{\text{biodieselconversion}(\%)} = \beta_0 + \sum_{j=1}^k \beta_j X_j + \sum_{j=1}^k \beta_{jj} X_j^2 + \sum_{i=1}^{j-1} \sum_{j=2}^k \beta_{ij} X_i X_j + \varepsilon \quad (2)$$

In Eq. 2, Y represents the predicted biodiesel conversion, k is the number of factors studied and optimized in the experiment, i and j are the linear and quadratic coefficients, X_i and X_j are the uncoded independent variables, β_0 is the regression coefficient, ε is the experimental error. Analysis of variance (ANOVA)—with a significance level of 5%—was used to validate the model. Moreover, the effect of independent process variables and their interactions on the biodiesel conversion were also studied by means of ANOVA. The probability error and statistical significance of the model were determined and tested by the p value. The interaction effects between independent reaction parameters as well as the optimal value of individual parameter having impact on the transesterification reaction were measured by expressing Eq. 2 as response surfaces.

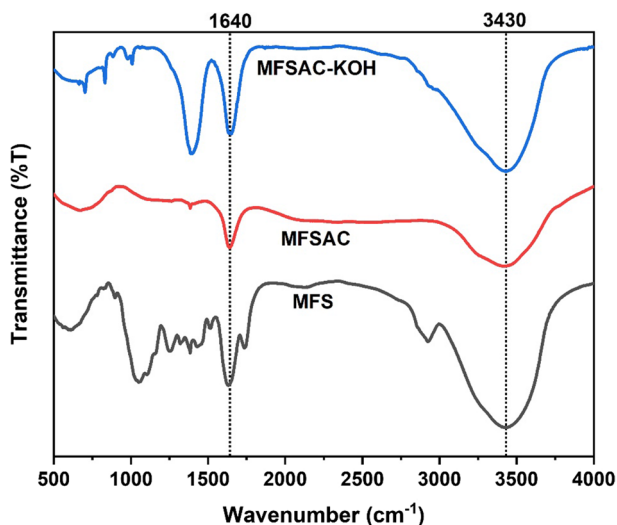


Fig. 1 FT-IR spectra of ball-milled raw Mahogany fruit shell (MFS), HCl-pretreated and carbonized MFS (MFSAC) and KOH-impregnated activated carbon (MFSAC-KOH) showing the presence of different functionalities

Results and discussion

Catalyst characterization

FT-IR analysis

The FT-IR spectra of MFS, MFSAC, and MFSAC-KOH are presented in Fig. 1. The broad band at 3430 cm^{-1} can be attributed to O–H stretching. The strong absorption band at 1640 cm^{-1} is responsible for C=C stretching [44]. On the other hand, the presence of bands at 1394 cm^{-1} and 1000 cm^{-1} can be attributed to C=O [45] and C–O stretching [46], respectively. It is noticeable that the bands responsible for C=O and C–O stretching are absent in MFSAC sample, owing to the fact that MFSAC was prepared in a tubular furnace under N_2 flow. Due to KOH impregnation, a band at 702 cm^{-1} corresponding to K–O stretching appears for MFSAC-KOH sample.

XRD analysis

The XRD patterns of MFSAC and MFSAC-KOH are presented in Fig. 2. A notable contrast between the spectra of MFSAC and MFSAC-KOH was observed. Broad diffraction peaks at $2\theta = 25.21^\circ$ and $2\theta = 42.45^\circ$ for MFSAC sample relate to typical amorphous carbon [47] and can be indexed to C (002) and C (100) planes, respectively, of the hexagonal graphite structure [48]. As a result of KOH loading, various diffraction peaks appeared at 24.10° , 29.98° , 31.18° , 34.02° , 39.14° , 40.42° , and

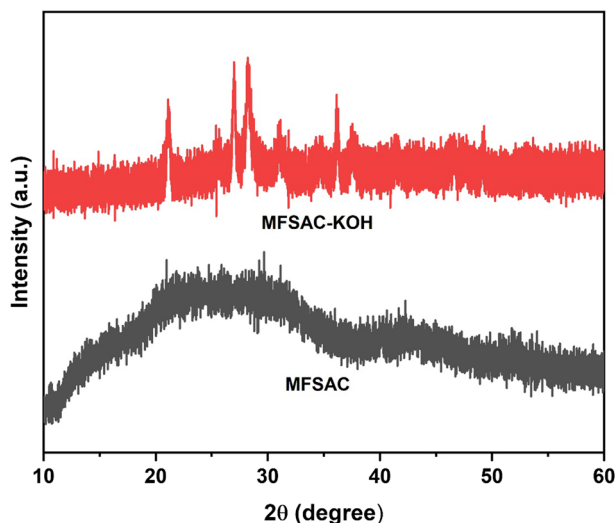


Fig. 2 XRD patterns of HCl-treated and carbonized (700 °C for 4 h) MFSAC and KOH-impregnated MFSAC-KOH catalyst synthesized after post-carbonization (850 °C for 2 h)

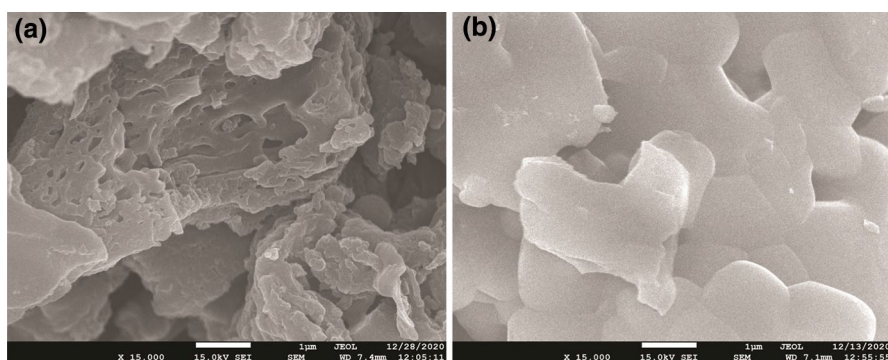


Fig. 3 FESEM images (scale bar: 1 μm) of **a** MFSAC and **b** MFSAC-KOH

52.30°. The peaks observed at $2\theta = 29.98^\circ$, 40.42° , and 52.30° correspond to the presence of K_2O [49].

FESEM-EDS analysis

Fig. 3a and b show the FESEM images of MFSAC and MFSAC-KOH. A significant extent of porosity owing to cracks and crevices can be observed on the surface of MFSAC [47]. Fig. 3b shows the presence of flakes-like substances stacked one over another, which has been caused by penetration and adsorption of KOH molecules on the surface of MFSAC. The EDS spectra and corresponding FESEM images of MFSAC and MFSAC-KOH samples are shown in Fig. 4a and b. EDS spectrum of

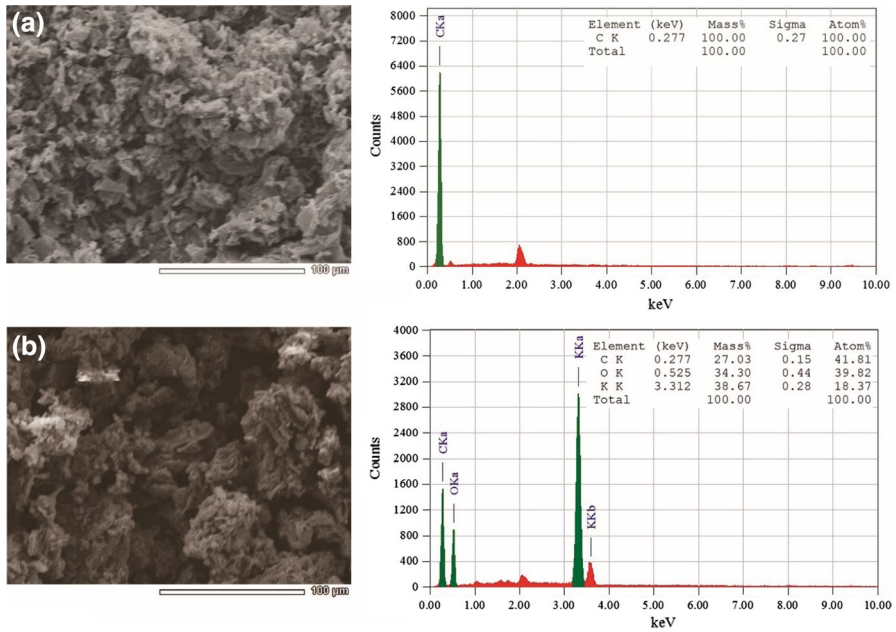


Fig. 4 FESEM images (left; scale bar: 100 μm) and EDS spectra (right) of **a** MFSAC and **b** MFSAC-KOH

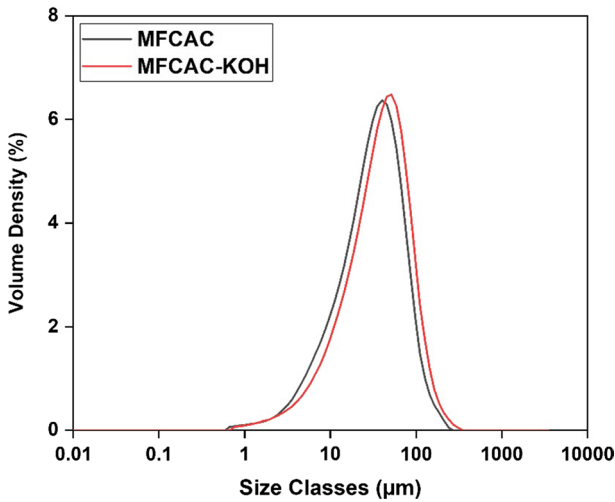


Fig. 5 Particle size distribution of MFSAC (laster obscuration: 7.81%, weighted residual: 1.15%) and MFSAC-KOH (laster obscuration: 6.60%, weighted residual: 0.92%) dispersed in deionized water

Table 2 Volume density and mean diameter parameters obtained from particle size analysis

Sample	Volume density				Mean		SSA (m ² /kg)	Uniformity
	Dv (10)	Dv (50)	Dv (90)	Dv (40)	D [2, 3]	D [3, 4]		
MFCAC	8.49	34.1	84.6	27.2	17.3	42.1	345.8	0.713
MFCAC-KOH	10.3	42.3	103	33.7	20.1	50.5	298.0	0.674

SSA specific surface area

MFSAC shows the presence of C (100 atom%) only. On the other hand, EDS spectrum of MFSAC-KOH shows the presence of C (41.81 atom %), O (39.82 atom %), and K (18.27 atom %), confirming the penetration of KOH molecules.

Particle size analysis

The overall particle size distribution of MFSAC and MFSAC-KOH is shown in Fig. 5. It can be seen that the particle size distribution for both samples are unimodal or normal. Other relevant parameters, such as volume density and mean obtained from particle size analysis were shown in Table 2. Dv (50), or the median value, splits the total population into two halves, with 50% particles having diameter below and 50% particles having diameter above this value. Similarly, Dv (90) implies the diameter below which diameter of 90% particles reside. It is interesting to observe that Dv (10), Dv (40), Dv (90) and Dv (40) values of

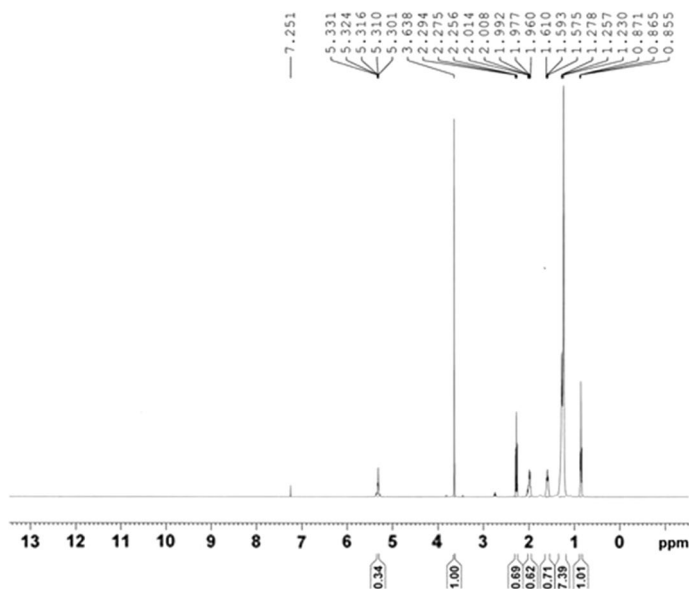


Fig. 6 ¹H-NMR spectrum of FAME from exp. 14 (experimental conditions: 2 wt% catalyst concentration, 12:1 methanol to oil molar ratio, 180 min reaction time and 65 °C reaction temperature)

Table 3 BBD matrix for transesterification involving three independent reaction parameters

Run	A: Catalyst concentration (wt%)	B: Methanol:oil (mol:mol)	C: Reaction time (min)	Experimental FAME yield (%)	Predicted FAME yield (%)
1	1.25	9	180	87.28	87.36
2	1.25	9	180	87.31	87.36
3	2	9	120	75.33	75.49
4	1.25	9	180	87.48	87.36
5	2	6	180	39.20	40.29
6	1.25	6	120	38.12	37.13
7	1.25	12	240	94.55	95.55
8	2	9	240	83.56	83.09
9	0.5	9	120	71.12	71.58
10	1.25	12	120	91.11	91.47
11	1.25	6	240	53.98	51.82
12	0.5	9	240	82.89	82.73
13	0.5	12	180	88.01	87.19
14	2	12	180	97.26	96.74
15	0.5	6	180	45.15	45.57

Table 4 Fit summary statistics of the linear model

S	R ² (%)	Adjusted R ² (%)	Predicted R ² (%)
0.977655	99.92	99.78	98.76

MFCAC-KOH are larger than those of MFCAC, implying that the diameter of MFCAC particles increase in general upon KOH impregnation. D [2, 3], or Sauter mean diameter, reflects the average diameter of fine particulates present in the sample. On the other hand, D [3, 4], or De Brouckere mean diameter, highlights the average diameter of coarse particulates that constitute the bulk of the sample population. Specific surface area and uniformity values of MFCAC-KOH sample decreased from those of MFCAC following the impregnation with KOH.

¹H-NMR analysis of the biodiesel

Biodiesel conversion (% of yield) was calculated following the formula given in Eq. 1. The ¹H-NMR spectrum (Fig. 6) of FAME from exp. 14 shows a strong singlet peak for the methoxy protons at 3.64 ppm. On the other hand, a triplet peak for the methylene protons was found to be present at 2.29 ppm. Absence of glycerol peaks in the range 4.00–4.20 ppm further affirms the formation of FAME [43, 50]. The biodiesel yield for exp. 14 was calculated to be 97.26%—the highest of all the experimental yields from 15 experiments. Some additional ¹H-NMR

spectra of FAME from high yield experiments have been provided in Supplementary Figs. S1–S4.

Response surface methodology analysis

Box–Behnken design experiments

Table 3 represents the experiments that were carried out following BBD matrix. The experimental data was found to be best fitted to a linear model. The relevant parameters associated with the model is presented in Table 4.

Regression analysis and analysis of variance

The R^2 (coefficient of determination), adjusted R^2 , and predicted R^2 values were found to be 99.92%, 99.78%, and 98.76% and are shown in Table 4. The high reliability of the model can be understood from the high R^2 value of 99.92%, indicating that the model obtained can explain 99.92% of variability. The adequacy and successful correlation of the obtained model with the process variables and response are confirmed by the high value of adjusted R^2 (99.78%). The small value (0.977655) of the standard error of regression (S) discloses the observed values to be in close proximity of the fitted line. The ANOVA for the suggested linear model is shown in Table 5. The fitted model can be termed statistically significant at 95%

Table 5 Statistical data of the BBD produced by ANOVA

Source	Degrees of freedom	Adjusted sum of squares	Adjusted mean square	F value	p value
Model	9	5949.71	661.08	691.64	0.000
Linear	3	4992.31	1664.10	1741.04	0.000
A	1	9.14	9.14	9.56	0.027
B	1	4807.39	4807.39	5029.66	0.000
C	1	175.78	175.78	183.91	0.000
Square	3	871.08	290.36	303.79	0.000
A ²	1	105.17	105.17	110.04	0.000
B ²	1	784.05	784.05	820.30	0.000
C ²	1	53.17	53.17	55.62	0.001
2-Way interaction	3	86.31	28.77	30.10	0.001
AB	1	54.98	54.98	57.52	0.001
AC	1	3.13	3.13	3.28	0.130
BC	1	28.20	28.20	29.50	0.003
Error	5	4.78	0.96		
Lack-of-fit	3	4.60	1.53	16.72	0.057
Pure error	2	0.18	0.09		
Total	14	5954.49			

interval because of having a very high *F* value (691.64) and the least possible *p* value (0.000). High significance of the regression coefficients is reflected by smaller *p* values [19]. Because of having *p* value less than 0.05, each process variable was concluded to be significant, with both methanol: oil ratio (*B*) and reaction time (*C*) showing the highest significance because of having least possible *p* values. Additionally, the model terms A^2 , B^2 , C^2 , *AB*, and *BC* were statistically significant as well, owing to their *p* values being less than 0.05. However, the term *AC*—because of having *p* value > 0.05—was considered non-significant. The predicted R^2 value of 98.76% and the lack of fit *p* value being non-significant (0.057) indicate that the model is good for the prediction purpose. The mathematical relationship between the yield and reaction parameters is expressed by the following equation (Eq. 3).

$$\begin{aligned} \text{Biodieselconversion}(\%) = & -191.94 + 13.86A + 37.91B + 36.89C - 9.488A^2 \\ & - 1.6191B^2 - 3.795C^2 + 1.648AB - 1.180AC - 0.885BC \end{aligned} \quad (3)$$

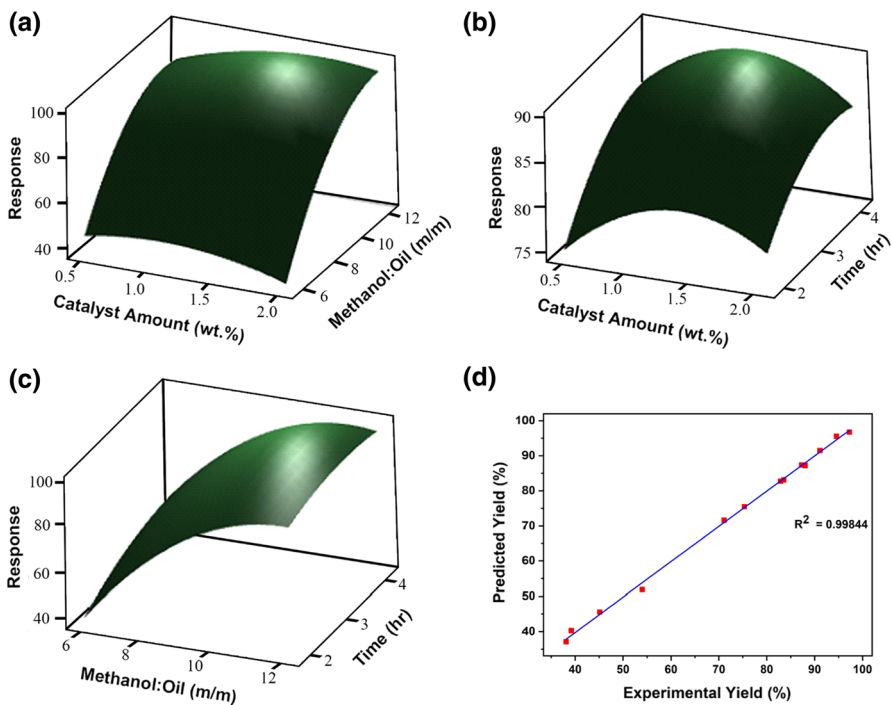


Fig. 7 Response surface plots for the interaction of **a** catalyst concentration and methanol to oil molar ratio, **b** catalyst concentration and time, **c** methanol to oil molar ratio and time and **d** linear regression plot for experimental yield vs. predicted yield

Effect of process variables on conversion efficiency

Interaction of catalyst concentration and methanol to oil ratio

The response surface plot (RSP) for the interaction between catalyst concentration (varied from 0.5 to 2 wt%) and methanol to oil ratio (varied from 6:1 to 12:1), with the reaction time being fixed at 180 min are presented in Fig. 7a. The plot reveals that methanol to oil ratio is more influential than the catalyst concentration on the biodiesel conversion. A close look at Fig. 7a and Table 3 reveals that at low methanol to oil ratio—irrespective of the catalyst concentration—the yield is always poor, with the lowest yield (39.20%) coming from exp. 5 at methanol to oil ratio of 6:1 and maximum catalyst concentration of 2 wt%. However, increasing the methanol amount increases the biodiesel yield dramatically, with the combination of methanol to oil ratio of 12:1 and catalyst concentration of 2 wt% (exp. 14) being responsible for the highest yield (97.26%). It has been reported that low methanol to oil molar ratio leads to poor mixing of the participating reactants in the transesterification process hence leading to poor biodiesel yield [19, 51]. Nevertheless, if the amount of methanol in the reaction mixture goes beyond the optimum level, the polarity of the reaction medium will increase. This phenomenon can make glycerol go into ester phase and reduce the yield by shifting the equilibrium toward the backward direction [52]. Additionally, excess methanol hinders the production of FAME and glycerol by flooding the active sites of the catalyst [10].

Interaction of catalyst concentration and reaction time

Fig. 7b highlights the interaction between catalyst concentration (varied from 0.5 to 2 wt%) and time (varied from 120 to 240 min) while keeping the methanol: oil fixed at 9:1. Approximately 40% biodiesel conversion was achieved for low catalyst concentration and shorter reaction time. Increasing the amount of catalyst increases the yield owing to the increased presence of the basic sites present in the catalyst. Nevertheless, catalyst amount beyond the optimal level will have a negative impact on the biodiesel yield owing to the increased viscosity of the reaction mixture leading to reduced mixing [53]. Increasing the reaction time increases the biodiesel yield depending upon the increase in the reaction times provided that methanol to oil ratio is adequately high enough. However, continuing the reaction for too long may result in poor yield by moving the reaction in the reverse direction [54].

Interaction of methanol to oil molar ratio and reaction time

Fig. 7c represents the 3D RSP for the interaction effects of methanol to oil ratio (varied from 6:1 to 12:1) and reaction time (varied from 120 to 240 min) on the yield. The catalyst concentration was fixed to be 1.25 wt%. Both methanol to oil ratio (p value=0.000) and reaction time (p value=0.000) have mentionable impact on the

conversion. For low methanol to oil ratio (6:1) and shorter reaction time (120 min), the yield is poor (38.12%), as evident from exp. 6. Increase in reaction time does not have a positive impact on the product yield if the methanol to oil ratio is kept low (6:1). On the contrary, even with a shorter reaction time of 120 min, the yield can still be pretty high (91.11%) for a high methanol to oil ratio (12:1) as evident from exp. 10. The biodiesel yield can be increased significantly when both the reaction time and methanol to oil ratio are increased simultaneously. However, increasing the reaction time beyond optimum, as already mentioned, can reverse the transesterification process. A closer look at Table 3 discloses that high yields from exp. 7 (94.55%), exp. 10 (91.11%), and exp. 14 (97.26%) were influenced mostly because of high methanol to oil molar ratio (12:1). ANOVA analysis and Table 5 reveal that methanol to oil molar ratio—owing to least possible p value (0.000) and very high F value (5029.66)—is the most significant term to influence and maximize the biodiesel conversion.

Optimum reaction conditions

According to BBD-based matrix presented in Table 3, a maximum yield of 96.74% was supposed to be achieved for a 180-min reaction done with 2 wt% of catalyst concentration and methanol to oil ratio of 12:1. The experimental yield—following the predicted parameters—for the same reaction (exp. 14) was found to be 97.26%. Fig. 7d shows that all the experimental yields were very close to the predicted yields, as suggested by the close-to-unity R^2 value of 0.99844.

Table 6 Comparison of MFSAC-KOH's performance with AC from other sources for biodiesel production from different feedstocks

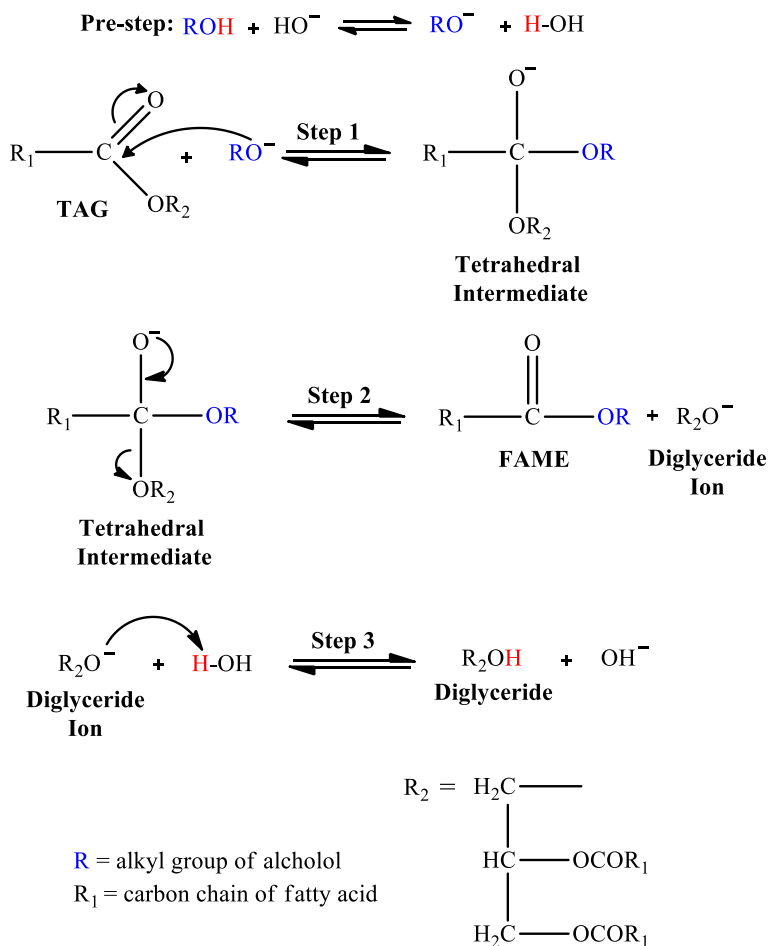
Impregnated material	Feedstock	Maximum conversion (%)	Catalyst concentration (wt%)	Methanol to oil ratio (molar)	Reaction time (min)	References
KOH	WCO	93.9	1.0	6:1	120	[10]
KOH	Jatropha oil	93.3	1.0	6:1	120	[10]
KOH	<i>Hevea brasiliensis</i> oil	89.3	3.5	15:1	60	[42]
NaOH/CaO	Soyabean oil	91.0	7.5	0.5:1 (M) ^a	180	[8]
KOH	Rapeseed oil	91.7	1.5	6:1	240	[11]
KOH	Sunflower oil	92.8	0.5	6:1	240	[11]
KOH	Corn oil	91.8	1.5	6:1	240	[11]
KOH	Olive oil	93.5	1.5	6:1	60	[11]
NaOH	WCO	98.9	10	1:2 (V) ^b	120	[39]
SrO	WCO	98.5	7.1	6:1	60	[40]
KOH	WCO	97.3	2	12:1	180	This study

^aMass ratio

^bVolumetric ratio

Performance analysis of MFSAC-KOH

MFSAC-KOH's performance as a heterogenous base catalyst has been compared with some other recently reported catalysts and reported in Table 6. As of late, Kamel et al. [10] and Narowska et al. [11] studied the catalytic efficiency of AC-KOH on biodiesel conversion from various feedstocks and the yields were found to be varied from 91.0 to 93.9%. Whereas, even though Niju et al. [39] and Tabah et al.'s [40] study on AC-NaOH and AC-SrO produced conversion above 98%, it was achieved at the expense of high catalyst concentration. Thus, it can be stated that MFSAC-KOH is a very efficient catalyst for delivering high conversion at a relatively low catalyst concentration and methanol to oil molar ratio for a 180-min-reaction. Additionally, the efficacy, if any, of catalyst support MFSAC as a catalyst with MFSAC-KOH system was also measured and compared. Using the same



Scheme 1 Mechanism of base catalyzed transesterification of TAG to biodiesel

optimum condition achieved using MFSAC-KOH catalyst, we ran a reaction using MFSAC only instead of MFSAC-KOH and found the yield to be very low (42.6%). The corresponding $^1\text{H-NMR}$ spectrum of the reaction yield can be found in Fig. S5. It is the nucleophilic character of the $\text{C}=\text{C}$ π -bonds and methanol that can give rise to the production of methoxide ions (CH_3O^-) to some extent to cause biodiesel with a very low yield.

Mechanism of base catalyzed transesterification

The mechanism of the activated carbon supported solid base catalyzed transesterification reaction has been outlined in Scheme 1. Initially (pre-step), an alcohol molecule (methanol in this case) gets adsorbed on the surface of the solid base catalyst to produce a catalytically active alkoxide ion (RO^-).

The nucleophile alkoxide ion attacks the carbonyl carbon of the TAG molecule to generate a tetrahedral intermediate. This intermediate then undergoes rearrangement to produce FAME and diglyceride ion. The diglyceride ion abstracts a proton from H_2O molecule to produce diglyceride and the base. The base molecule then attacks the diglyceride molecule, thereby starting a new catalytic cycle.

FAME composition analysis

Table 7 contains the FAME composition achieved through GC analysis. Mono-unsaturated methyl oleate (C18:1; 48.19%) and saturated methyl palmitate (C16:0; 41.18%) were found to be the major composition of FAME, with some minor saturated and unsaturated components, such as methyl linoleate (C18:2), methyl stearate (C18:0), methyl myristate (C14:0), etc. also being present. However, the total composition of FAME was found to be greater than 95%, which is in compliance with EN 14214. This actually confers the notion that MFSAC-KOH is capable in the transesterification of almost all the fatty acids present in the TAG feedstock. It is also worth mentioning that, based on the limit set by EN 14214, the composition of polyunsaturated methyl esters with more than four double bonds should not exceed 1 wt% as the biodiesel sample would be highly viscous otherwise [40]. The

Table 7 FAME composition from GC analysis

FAME name	FAME component	FAME concentration (% w/w)
Laurate	C12:0	0.76
Myristate	C14:0	1.20
Palmitate	C16:0	41.18
Stearate	C18:0	1.67
Oleate	C18:1	48.19
Linoleate	C18:2	6.11
Linolenate	C18:3	0.02
Arachidate	C20:0	0.22
Eicosenoate	C20:1	0.34

Table 8 Physicochemical properties of the synthesized biodiesel

Parameters	Measured value	EN 14214	ASTM D6751	Test method
Viscosity (cSt) ^a	4.58	3.50–5.00	1.9–6.0	ASTM D445
Density (kg/m ³) ^b	862	860–890	860–890	ASTM D4052
Calorific value (KJ/kg)	39,102	–	–	ASTM D240
Acid value (mg KOH/g)	0.28	0.50 max	0.8 max	ASTM D664
Pour point (°C)	16.0	–	–	ASTM D97
Flash point (°C)	128	120 min	130 min	ASTM D93

^aMeasured at 40 °C

^bmeasured at 25 °C

synthesized biodiesel under study does not contain any methyl ester component with even four double bonds, indicating that the synthesized biodiesel is highly comparable to conventional petrodiesel in terms of viscosity.

Properties analysis of biodiesel

Table 8 represents different physicochemical properties of the produced biodiesel. The properties were compared with ASTM and EN standards and found to be in good agreement. The lower value of kinematic viscosity indicates that the biodiesel can be used in existing engines, whereas, high flash point indicates the safety and transportability of the prepared biodiesel. The calorific value was found to be a bit higher than other reported biodiesels but lower than conventional petrol diesel. Furthermore, the acid value was found to be lower than the maximum allowed value, meaning that it's safe for fuel tank and diesel engine parts. Therefore, the synthesized biodiesel is safe for use—either directly or by blending with petrodiesel.

Conclusion

The objectives of this study were met by developing KOH impregnated activated carbon (MFSAC-KOH) from widely available biomass source Mahogany fruit shell and employ it as a base catalyst for the transesterification of environment pollutant WCO to green biodiesel. FT-IR, XRD, FESEM-EDS and particle size analysis techniques provided significant details about MFSAC and MFSAC-KOH samples. BBD-based RSM was utilized to optimize the process parameters of the transesterification reaction. A maximum of 97.26% biodiesel yield was achieved following the optimized conditions of 2 wt% catalyst concentration, 12:1 methanol to oil ratio and 180-min reaction time. Among all process parameters, methanol to oil molar ratio played the most important role in deciding the extent of biodiesel yield. Physicochemical parameters of the synthesized biodiesel conferred that it is safe for use, storage and transportation. The as-prepared MFSAC-KOH solid base catalyst may have potential implications in the transesterification of other TAG feedstocks.

Supplementary Information The online version contains supplementary material available at <https://doi.org/10.1007/s11144-021-01995-w>.

Acknowledgements The authors would like to thank Mr. Farid Ahmed, Institute of Glass and Ceramics Research and Testing (IGCRT), BCSIR, Dhaka-1205, Bangladesh, for his help with particle size analysis. The authors are thankful to Dr. Abdul Gafur, Pilot Plant and Process Development Center (PP & PDC), BCSIR, Dhaka-1205, Bangladesh, for his assistance with XRD analysis. The authors gratefully acknowledge the research facilities provided by Institute of Fuel Research and Development (IFRD), BCSIR, Dhaka-1205, Bangladesh.

Author contributions MH: Conceptualization, methodology, software, formal analysis, investigation, visualization. LKMOG: Validation, writing—original draft, visualization. NM: Writing—original draft. MSJ: Writing—review and editing, visualization. SMAS: Project administration. SA: Resources. DI: Resources. RHB: Resources. ANMF: Supervision.

Funding No funds, grants, or other support was received.

Data availability The datasets generated during and/or analysed during the current study are available from the corresponding author on reasonable request.

Declarations

Conflicts of interest The authors have no conflicts of interest to declare that are relevant to the content of this article.


References

1. Shafiee S, Topal E (2009) When will fossil fuel reserves be diminished? *Energy Policy* 37:181–189
2. Proadhan A, Hasan MI, Sujon SMA et al (2020) Production and characterization of biodiesel from *Jatropha* (*Jatropha curcas*) seed oil available in Bangladesh. *Energy Sources Part A* 42:1–16
3. Samanta S, Sahoo RR (2020) Waste cooking (palm) oil as an economical source of biodiesel production for alternative green fuel and efficient lubricant. *Bioenergy Res* 14:163–174
4. Bhatia SK, Gurav R, Choi TR et al (2020) Conversion of waste cooking oil into biodiesel using heterogeneous catalyst derived from cork biochar. *Bioresour Technol* 302:1–6
5. Kumar U, Gupta P (2020) Modeling and optimization of novel biodiesel production from non-edible oil with *Musa balbisiana* root using hybrid response surface methodology along with african buffalo optimization. *React Kinet Mech Catal* 130:875–901
6. Ramos M, Soares Dias AP, Teodoro F (2020) Soybean oil ethanolysis over Ca based catalyst. Statistical optimization of reaction conditions. *React Kinet Mech Catal* 130:433–445
7. Alam MJ, Rana SMS, Haque MA et al (2017) Biodiesel from non-edible *Karanja* seed oil. *Bangladesh J Sci Ind Res* 52:15–20
8. Faria DN, Cipriano DF, Schettino MA et al (2020) Na, Ca-based catalysts supported on activated carbon for synthesis of biodiesel from soybean oil. *Mater Chem Phys* 249:1–9
9. Ganesan S, Nadarajah S, Shamsudin NN et al (2020) Esterification of palm fatty acid distillate using ammonium ferric sulfate-calcium silicate as a heterogeneous acid catalyst. *Bioenergy Res* 13:1297–1307
10. Kamel DA, Farag HA, Amin NK, Fouad YO (2017) Biodiesel synthesis from non-edible oils by transesterification using the activated carbon as heterogeneous catalyst. *Int J Environ Sci Technol* 14:785–794
11. Narowska BE, Kułczyński M, Łukaszewicz M (2020) Application of activated carbon to obtain biodiesel from vegetable oils. *Catalysts* 10:1–14
12. Ogbu IM, Ajiwe VIE, Okoli CP (2018) Performance evaluation of carbon-based heterogeneous acid catalyst derived from *Hura crepitans* seed pod for esterification of high FFA vegetable oil. *Bioenergy Res* 11:772–783

13. Pua F, Fang Z, Zakaria S et al (2012) Direct production of biodiesel from high-acid value *Jatropha* oil with solid acid catalyst derived from lignin. *Biotechnol Biofuels* 5:1–8
14. Alkhafaje ZA, Mohammed AK, Rashid IM (2020) Development of two-step noncatalytic esterification of waste cooking oil for biodiesel preparation. *React Kinet Mech Catal* 131:645–659
15. Mofijur M, Masjuki HH, Kalam MA et al (2013) Effect of biodiesel from various feedstocks on combustion characteristics engine durability and materials compatibility: a review. *Renew Sustain Energy Rev* 28:441–455
16. Ayetor GK, Sunnu A, Parbey J (2015) Effect of biodiesel production parameters on viscosity and yield of methyl esters: *Jatropha curcas*, *Elaeis guineensis* and *Cocos nucifera*. *Alexandria Eng J* 54:1285–1290
17. Carlini M, Castellucci S, Cocchi S (2014) A pilot-scale study of waste vegetable oil transesterification with alkaline and acidic catalysts. *Energy Procedia* 45:198–206
18. Ashrafal AM, Masjuki HH, Kalam MA et al (2014) Production and comparison of fuel properties, engine performance, and emission characteristics of biodiesel from various non-edible vegetable oils: a review. *Energy Convers Manag* 80:202–228
19. Niju S, Rabia R, Sumithra Devi K et al (2020) Modified *Malleus malleus* shells for biodiesel production from waste cooking oil: an optimization study using Box-Behnken design. *Waste Biomass Valoriz* 11:793–806
20. Mansir N, Teo SH, Rabi I, Taufiq-Yap YH (2018) Effective biodiesel synthesis from waste cooking oil and biomass residue solid green catalyst. *Chem Eng J* 347:137–144
21. Mayorga Betancourt MA, López Santamaria CA, López Gómez M, Gonzalez Caranton AR (2020) Experimental analysis of biodiesel synthesis from palm kernel oil: empirical model and surface response variables. *React Kinet Mech Catal* 131:297–317
22. Mandolesi De Araújo CD, De Andrade CC, De Souza E, Silva E, Dupas FA (2013) Biodiesel production from used cooking oil: a review. *Renew Sustain Energy Rev* 27:445–452
23. Torres-Rodríguez DA, Romero-Ibarra IC, Ibarra IA, Pfeiffer H (2016) Biodiesel production from soybean and *Jatropha* oils using cesium impregnated sodium zirconate as a heterogeneous base catalyst. *Renew Energy* 93:323–331
24. Yaakob Z, Mohammad M, Alherbawi M et al (2013) Overview of the production of biodiesel from waste cooking oil. *Renew Sustain Energy Rev* 18:184–193
25. Shan R, Lu L, Shi Y et al (2018) Catalysts from renewable resources for biodiesel production. *Energy Convers Manag* 178:277–289
26. Hadiyanto H, Afianti AH, Navi'a UI, et al (2017) The development of heterogeneous catalyst C/CaO/NaOH from waste of green mussel shell (*Perna varidis*) for biodiesel synthesis. *J Environ Chem Eng* 5:4559–4563
27. Roschat W, Siritanon T, Yoosuk B, Promarak V (2016) Rice husk-derived sodium silicate as a highly efficient and low-cost basic heterogeneous catalyst for biodiesel production. *Energy Convers Manag* 119:453–462
28. Dhawane SH, Kumar T, Halder G (2018) Recent advancement and prospective of heterogeneous carbonaceous catalysts in chemical and enzymatic transformation of biodiesel. *Energy Convers Manag* 167:176–202
29. Gupta VK, Nayak A, Bhushan B, Agarwal S (2015) A critical analysis on the efficiency of activated carbons from low-cost precursors for heavy metals remediation. *Crit Rev Environ Sci Technol* 45:613–668
30. Sartape AS, Patil SA, Patil SK et al (2015) Mahogany fruit shell: a new low-cost adsorbent for removal of methylene blue dye from aqueous solutions. *Desalin Water Treat* 53:99–108
31. Kader MA, Joardder MUH, Islam MR et al (2012) Production of liquid fuel and activated carbon from Mahogany seed by using pyrolysis technology. In: *Green chemistry for sustainable development*. Elsevier, London, pp 1–6
32. Rana S, Haque M, Poddar S et al (2015) Biodiesel production from non-edible Mahogany seed oil by dual step process and study of its oxidation stability. *Bangladesh J Sci Ind Res* 50:77–86
33. Kumar M, Sharma MP (2016) Optimization of transesterification of *Chlorella protothecoides* oil to biodiesel using Box–Behnken design method. *Waste Biomass Valoriz* 7:1105–1114
34. Rashtizadeh E, Farzaneh F, Talebpour Z (2014) Synthesis and characterization of $\text{Sr}_3\text{Al}_2\text{O}_6$ nanocomposite as catalyst for biodiesel production. *Bioresour Technol* 154:32–37
35. Magoling BJA, Macalalad AA (2017) Optimization and response surface modelling of activated carbon production from Mahogany fruit husk for removal of chromium (VI) from aqueous solution. *BioResources* 12:3001–3016

36. Patil SA, Suryawanshi UP, Harale NS et al (2020) Adsorption of toxic Pb (II) on activated carbon derived from agriculture waste (Mahogany fruit shell): isotherm, kinetic and thermodynamic study. *Int J Environ Anal Chem* 100:1–17
37. Alsultan A, Mijan A, Yap T (2016) Preparation of activated carbon from walnut shell doped La and Ca catalyst for biodiesel production from waste cooking oil. *Mater Sci Forum* 840:348–352
38. Buasri A, Ksapabutr B, Panapoy M, Chaiyut N (2012) Biodiesel production from waste cooking palm oil using calcium oxide supported on activated carbon as catalyst in a fixed bed reactor. *Korean J Chem Eng* 29:1708–1712
39. Niju S, Ajieth Kanna SK, Ramalingam V et al (2019) Sugarcane bagasse derived biochar—a potential heterogeneous catalyst for transesterification process. *Energy Sources Part A* 41:1–12
40. Tabah B, Nagvenkar AP, Perkas N, Gedanken A (2017) Solar-heated sustainable biodiesel production from waste cooking oil using a sonochemically deposited SrO catalyst on microporous activated carbon. *Energy sFuels* 31:6228–6239
41. Narowska B, Kułażyński M, Łukasiewicz M, Burchacka E (2019) Use of activated carbons as catalyst supports for biodiesel production. *Renew Energy* 135:176–185
42. Dhawane SH, Kumar T, Halder G (2015) Central composite design approach towards optimization of flamboyant pods derived steam activated carbon for its use as heterogeneous catalyst in transesterification of *Hevea brasiliensis* oil. *Energy Convers Manag* 100:277–287
43. Gelbard G, Brès O, Vargas RM et al (1995) ^1H nuclear magnetic resonance determination of the yield of the transesterification of rapeseed oil with methanol. *J Am Oil Chem Soc* 72:1239–1241
44. Kamalini A, Muthusamy S, Ramapriya R et al (2018) Optimization of sugar recovery efficiency using microwave assisted alkaline pretreatment of cassava stem using response surface methodology and its structural characterization. *J Mol Liq* 254:55–63
45. Ramadoss G, Muthukumar K (2015) Influence of dual salt on the pretreatment of sugarcane bagasse with hydrogen peroxide for bioethanol production. *Chem Eng J* 260:178–187
46. Saleh TA, Al-Saadi AA, Gupta VK (2014) Carbonaceous adsorbent prepared from waste tires: experimental and computational evaluations of organic dye methyl orange. *J Mol Liq* 191:85–91
47. Fadhil AB, Aziz AM, Altamer MH (2018) Optimization of methyl esters production from non-edible oils using activated carbon supported potassium hydroxide as a solid base catalyst. *Arab J Basic Appl Sci* 25:56–65
48. Saleh TA (2011) The influence of treatment temperature on the acidity of MWCNT oxidized by HNO_3 or a mixture of $\text{HNO}_3/\text{H}_2\text{SO}_4$. *Appl Surf Sci* 257:7746–7751
49. Lin YC, Yang PM, Chen SC, Lin JF (2013) Improving biodiesel yields from waste cooking oil using ionic liquids as catalysts with a microwave heating system. *Fuel Process Technol* 115:57–62
50. Borah MJ, Devi A, Borah R, Deka D (2019) Synthesis and application of Co doped ZnO as heterogeneous nanocatalyst for biodiesel production from non-edible oil. *Renew Energy* 133:512–519
51. Tan YH, Abdullah MO, Nolasco-Hipolito C, Taufiq-Yap YH (2015) Waste ostrich- and chicken-eggshells as heterogeneous base catalyst for biodiesel production from used cooking oil: catalyst characterization and biodiesel yield performance. *Appl Energy* 160:58–70
52. Issariyakul T, Dalai AK (2014) Biodiesel from vegetable oils. *Renew Sustain Energy Rev* 31:446–471
53. Tshizanga N, Aransiola EF, Oyekola O (2017) Optimisation of biodiesel production from waste vegetable oil and eggshell ash. *S Afr J Chem Eng* 23:145–156
54. Niju S, Begum KMMS, Anantharaman N (2014) Preparation of biodiesel from waste frying oil using a green and renewable solid catalyst derived from egg shell. *Environ Prog Sustain Energy* 33:676–680

Authors and Affiliations

Mosharof Hossain^{1,2}  · **Lipiar Khan Mohammad Osman Goni²** ·
Nuzhat Muntaha² · **Mohammad Shah Jamal²** ·
Shah Mohammad Asaduzzaman Sujan² · **Shamim Ahmed³** · **Dipa Islam⁴** ·
Riyadh Hossen Bhuiyan⁵ · **Abu Naieum Muhammad Fakhruddin¹**

¹ Department of Environmental Sciences, Jahangirnagar University, Savar, Dhaka 1342, Bangladesh

² Institute of Fuel Research and Development, Bangladesh Council of Scientific and Industrial Research (BCSIR), Dhaka 1205, Bangladesh

³ Institute of National Analytical Research and Service, Bangladesh Council of Scientific and Industrial Research (BCSIR), Dhaka 1205, Bangladesh

⁴ Biomedical and Toxicological Research Institute, Bangladesh Council of Scientific and Industrial Research (BCSIR), Dhaka 1205, Bangladesh

⁵ Fiber and Polymer Research Division, Bangladesh Council of Scientific and Industrial Research (BCSIR), Dhaka 1205, Bangladesh